LINE DETECTION IN SPECKLE IMAGES USING RADON TRANSFORM AND ℓ_1 REGULARIZATION

Nantheera Anantrasirichai[1], *Marco Allinovi*[2], *Wesley Hayes*[3], *David Bull*[1], *Alin Achim*[1]

[1]Visual Information Lab, University of Bristol, Bristol, UK
[2]Paediatric Nephrology Unit, Meyer Childrens Hospital, Florence, Italy
[3]Great Ormond Street Hospital, London, UK

ABSTRACT

Boundaries and lines in medical images are important structures as they can delineate between tissue types, organs, and membranes. Although, a number of image enhancement and segmentation methods have been proposed to detect lines, none of these have considered line artefacts, which are more difficult to visualise as they are not physical structures, yet are still meaningful for clinical interpretation. This paper presents a novel method to restore lines, including line artefacts, in speckle images. We address this as a sparse estimation problem using a convex optimisation technique based on a Radon transform and sparsity regularisation (ℓ_1 norm). This problem divides into subproblems which are solved using the alternating direction method of multipliers, thereby achieving line detection and deconvolution simultaneously. The results for both simulated and in vivo ultrasound images show that the proposed method outperforms existing methods, in particular for detecting B-lines in lung ultrasound images, where the performance can be improved by up to 30 %.

***Index Terms*—** ultrasound, inverse problem, ADMM, line detection, sparsity regularisation

1. INTRODUCTION

Medical ultrasound (US) image quality is degraded heavily by speckle noise, which has a granular appearance related to limitations in spatial-frequency bandwidth of the interference signals. Detecting structures and lines in these speckle images is challenging due to the multiplicative noise causing multiple false peaks generated from collinear noisy edge points. Edge detection using local filtering or line detection using a Hough transform is consequently almost impossible without pre-processing to enhance the image and reduce speckle noise.

Several techniques have been proposed to deal specifically with speckle noise [1], while other techniques have focused on line detection in noisy images. Lee and Kweon employed Deriche's edge operator, which was claimed to be more robust to noise effects than other operators such as Sobel and Difference of Gaussian filters [2]. Eight directional sticks were employed in a technique by Czerwinski et al. [3] that used a rotating kernel transformation to enhance lines and curves in US images. A soft-threshold wavelet method was employed in [4] to remove noise while applying the Sobel edge detection before a Hough transform. These techniques generally require several pre-defined thresholds and parameters and are hence unreliable for use with data collected in different settings.

An important clinical application of line detection in speckle is B-line detection from lung ultrasound images. Physiologically, the difference in acoustic impedance between the lung and the surrounding tissues is increased when lung density increases due to transudate. This creates discrete hyper-echogenic reverberation artefacts arising from the pleural line, known as B-lines. The number of B-lines has positive linear correlation with extravascular lung water, so multiple B-lines are considered a sign of fluid overload [5]. A key challenge in the detection of B-lines is operator dependency, where identification and quantification of B-lines can be variable between different operators. Therefore, image processing techniques that improve the visibility of lines and facilitate line detection in speckle images are essential.

In this paper, we propose a novel solution to an inverse problem for line detection in speckle ultrasound (US) images, which also works well with line artefacts. We employ a Radon transform, where a grayscale image is converted to a representation of radius and orientation as shown in Fig. 1. This inverse problem is solved using the alternating direction method of multipliers (ADMM) [6], offering a fast convergence rate. We employ ℓ_1 regularisation since the nature of ℓ_1 norm is a convex relaxation of ℓ_0, which leads to sparsity. This obviously fits well with our work since the space of lines is sparse. We show results of line restoration in both simulated US images and in vivo B-mode US images. The automated B-line detection method [7] was applied to the results in order to investigate the performance in real applications.

The remainder of this paper is organised as follows. The

This work was supported in part by the Wellcome Trust Institutional Strategic Support Fund and the Elizabeth Blackwell Institute at the University of Bristol.

proposed line detection method is described in Section 2. The performance of the method is evaluated in Section 3. Finally, Section 4 presents the conclusions of this work.

2. PROPOSED LINE DETECTION IN SPECKLE IMAGES

Lines in speckle images can be described using the model

$$y = \mathcal{HC}x + n, \tag{1}$$

where y is the observed speckle image, x is the line represented by the orientation θ and distance r from the centre of y. $\mathcal{H}$ is a point spread function (PSF) generated in the imaging systems as ultrasounds in this case. $\mathcal{R}$ and $\mathcal{C}$ are a Radon transform and an inverse Radon transform, respectively. To operate with an image, $\mathcal{R}$ and $\mathcal{C}$ are discrete and can be implemented as proposed in [8]. n is Gaussian noise.

2.1. Optimisation problem

Eq. 1 can be seen as two separate subproblems which can be solved with two optimisation processes. The first process is to estimate the tissue reflectivity function (TRF) w from the blurred speckle image $y = \mathcal{H}w$, using Eq. 2.

$$\hat{w} = \arg\min_{w}\{||y - \mathcal{H}w||_2^2 + \alpha||w||_1\}. \tag{2}$$

The second process is to estimate the lines in the Radon transform domain x from the TRF $w = \mathcal{C}x$, using Eq. 3.

$$\hat{x} = \arg\min_{x}\{||\hat{w} - \mathcal{C}x||_2^2 + \beta||x||_1\}. \tag{3}$$

Solving two optimisation problems separately is computationally inefficient; therefore, we estimate x and w simultaneously by solving the following optimisation problem:

$$\hat{x} = \arg\min_{x}\{||y - \mathcal{HC}x||_2^2 + \alpha||\mathcal{C}x||_1 + \beta||x||_1\}. \tag{4}$$

2.2. Implementation

The ADMM [6] is employed to solve the problem in Eq. 4. It is a variant of the augmented Lagrangian scheme that uses partial updates for the dual variables. It is simple to implement by splitting a large problem into a series of subproblems as follows.

$$\begin{aligned} &\text{minimize } \; f(u) + g(v), \\ &\text{subject to } \; \mathcal{A}u - \mathcal{B}v = 0. \end{aligned} \tag{5}$$

where

$$f(u) = ||y - \mathcal{H}u||_2^2, \; u = w = \mathcal{C}x, \tag{6a}$$

$$g(v) = \alpha||w||_1 + \beta||x||_1, \; v = [w \; x]^T, \tag{6b}$$

$$\mathcal{A} = \begin{bmatrix} \mathcal{I} \\ \mathcal{I} \end{bmatrix}, \; \mathcal{B} = \begin{bmatrix} \mathcal{I} & 0 \\ 0 & \mathcal{C} \end{bmatrix}. \tag{6c}$$

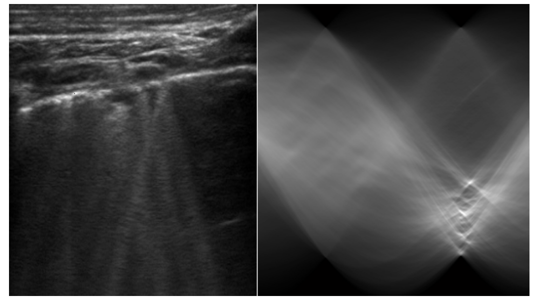

Fig. 1. Example of lung US image y (left) and its Radon transform $\mathcal{R}y$ (right), where the horizontal axis is θ varying from -45° to 135°, the vertical axis is r varying from $-r_{max}$ to r_{max}, and the brighter intensity indicates higher magnitude of the Radon transform.

u^T indicates the transpose of u, and $\mathcal{I}$ is an identity matrix with the same size as y, which is $N \times N$. Then, the Augmented Lagrangian for Eq. 5 is

$$\begin{aligned} \mathcal{L}_\rho(u, v, z) = {} & ||y - \mathcal{H}u||_2^2 + \alpha||w||_1 + \beta||x||_1 \\ & + z^T(\mathcal{A}u - \mathcal{B}v) + \frac{\rho}{2}||\mathcal{A}u - \mathcal{B}v||_2^2, \end{aligned} \tag{7}$$

where $z = [z_1 \; z_2]^T$ is the dual variable or Lagrange multiplier, $z_1 \in \mathbb{R}^{N\times N}$, $z_2 \in \mathbb{R}^{N\times N}$. $\rho > 0$ is a penalty parameter. The ADMM technique allows this problem to be solved approximately using three-step iterations, namely i) u-minimisation, ii) v-minimisation, and iii) dual update, as

$$u^{k+1} := \arg\min_{u} \mathcal{L}_\rho(u, v^k, z^k), \tag{8a}$$

$$v^{k+1} := \arg\min_{v} \mathcal{L}_\rho(u^{k+1}, v, z^k), \tag{8b}$$

$$z^{k+1} := z^k + \rho(\mathcal{A}u^{k+1} - \mathcal{B}v^{k+1}). \tag{8c}$$

where k is an internal iteration counter. As $v = [w \; x]^T$, the problem in Eq. 8b can be divided into two subproblems to restore w^{k+1} and x^{k+1} independently. The algorithm stops with the convergence criterion $||x^{k+1} - x^k||/||x^k|| < \epsilon$, where ϵ is a very small number (we use $\epsilon = 10^{-3}$ in this paper).

2.2.1. *Solving u^{k+1}*

The problem in Eq. 8a is a quadratic function about u, which can be solved as follows.

$$\begin{aligned} u^{k+1} = {} & \arg\min_{u} \; ||y - \mathcal{H}u||_2^2 + (z^k)^T(\mathcal{A}u - \mathcal{B}v^k) \\ & + \frac{\rho}{2}||\mathcal{A}u - \mathcal{B}v^k||_2^2, \\ = {} & (2\mathcal{H}^T\mathcal{H} + 2\rho\mathcal{I})^{-1}(2\mathcal{H}^Ty + \rho w^k + \rho\mathcal{C}x^k \\ & - z_1^k - z_2^k). \end{aligned} \tag{9}$$

2.2.2. *Solving w^{k+1} in v^{k+1}*

We define $\lambda_1 = \alpha/\rho$. The subproblem of Eq. 8b for w^{k+1} is a form of proximal operator of $\lambda_1||w||_1$ [9] and w^{k+1} can be computed as follows.

$$w^{k+1} = \arg\min_{w} \ \lambda_1 ||w||_1 + \frac{1}{2}||u^{k+1} - w + \frac{z_1^k}{\rho}||_2^2, \\ = S_{\lambda_1}\left(u^{k+1} + \frac{z_1^k}{\rho}\right), \tag{10}$$

where $S_\lambda(\bullet)$ is a soft thresholding described by

$$S_\lambda(a) = sign(a)\max(|a| - \lambda, 0). \tag{11}$$

2.2.3. Solving x^{k+1} in v^{k+1}

We define $\lambda_2 = \beta/\rho$. The subproblem of Eq. 8b for x^{k+1} is

$$x^{k+1} = \arg\min_{x} \ \lambda_2||x||_1 + \frac{1}{2}||u^{k+1} - \mathcal{C}x + \frac{z_2^k}{\rho}||_2^2. \tag{12}$$

We solve this problem using two-step iterative shrinkage/thresholding (TwIST) [10]. This method offers fast convergence rate for ill-conditioned problems. Starting with $\breve{x}^0 = x^k$, the iterative process proceeds as follows.

$$d = \breve{x}^t + \mathcal{R}\left(u^{k+1} - \mathcal{C}\breve{x}^t + \frac{z_2^k}{\rho}\right), \tag{13a}$$

$$\breve{x}^{t+1} = (1-\varrho)\breve{x}^{t-1} - \varrho\breve{x}^t + 2\varrho\mathcal{S}_{\lambda_2}(d), \tag{13b}$$

$$\mathcal{S}_{\lambda_2}(d) = \frac{\max(|d| - \lambda_2, 0)}{(\max(|d| - \lambda_2, 0) + \lambda_2)}d, \tag{13c}$$

where ϱ is a two-step parameter, defined as in [10]. t is an internal iteration counter, and $\lambda_2 > 0$. The iteration process stops when $||\breve{x}^{t+1} - \breve{x}^t||/||\breve{x}^t|| < \epsilon$, $x^{k+1} = \breve{x}^{t_{final}}$.

2.2.4. Computing z^{k+1}

The last step in each iteration is for updating z, which is

$$z_1^{k+1} = z_1^k + \rho(u^{k+1} - w^{k+1}), \tag{14a}$$

$$z_2^{k+1} = z_2^k + \rho(u^{k+1} - \mathcal{C}x^{k+1}) \tag{14b}$$

3. RESULTS AND DISCUSSION

We tested our proposed method with simulated speckle images and in vivo B-mode images. Then, the accuracy of the line restoration was examined with an automatic B-line detection method. We set α, β and ρ equal to 1.

3.1. Simulated speckle images

We created a simulated image (300×300 pixels) with several lines rotated at different angles as shown in Fig 2 (a) (The line image is on the top row and its Radon transform is on the bottom row). Subsequently, random multiplicative noise was added and the convolution with the simulated US PSF was applied, as used in [11]. The B-mode simulated image is shown in Fig. 2 (b). We compared our proposed method with three existing techniques: i) enhanced lines and boundaries of speckle images using sticks (STICKS) [3], ii) despeckling approach with adaptive-weighted bilateral filtering (AWBF) [12], and iii) line detection with log regularised Hough transform (HOUGH) [13]. Fig. 2 (c)-(f) show the restored line images (top row) and the Radon transforms (bottom row) of the STICKS, AWBF, HOUGH and the proposed method, respectively.

To detect lines, a local-maximum operator was applied to find local peaks $x(r_{peak}, \theta_{peak})$ in the Radon transform (marked with the plus signs, $+$, in the figure). These points were back-projected to the image domain y using the inverse Radon transform. Unfortunately, the back-projection does not contain information of the line length. Hence, we estimated the length using intensity values of $y(i,j), \{i,j\} \in \mathcal{C}x(r_{peak}, \theta_{peak})$ after applying a low-pass filter. The longest continuous line was drawn at the locations, where $y(i,j) > \bar{y}$ and $\bar{y}$ is the mean intensity value of the line. The results in Fig. 2 reveals that our proposed method and HOUGH can achieve good line detection as all lines can be identified correctly. Three lines were excluded in the raw speckle image, and one line was missed out by both AWBF and STICKS.

3.2. In vivo images – Lung ultrasounds

We examined the performance of our line detection approach for a real application in clinical practice – B-line detection. We estimate the PSF using the method proposed in [14]. We employed the B-line detection algorithm proposed in [7] (Section 3.2) to automatically count the number of B-lines in lung ultrasound images. Briefly, this algorithm detects the line artefacts in a Radon transform domain using a local maxima detection method. The pleural, A-, B- and Z-lines are detected within a range of orientations, where these artefacts could occur. The Z-lines can be seen as similar to the B-lines in the Radon transform, but they are erased by the A-lines. Then, the type of the line artefacts are classified following their clinical definitions. Fig. 3 shows the cropped areas underneath the pleural lines, where A-, B- and Z-lines appear, with the marks of the detected lines. The B-lines are counted as one if they originate from the same point on the pleural line – (seen as the merging point on the top of the cropped images). We compared our proposed method with HOUGH [13], which gave the best performance amongst the existing methods employed in the previous section.

In Fig. 3, the A-, B-, and Z-lines are drawn with red, yellow and green, respectively. The image on the left, (a1)-(c1), contains five horizontal A-lines, one vertical B-line and one Z-line going across the A-lines. This ground truth was confirmed by clinical experts. The proposed method can detect all lines correctly, whilst HOUGH misses two A-lines since the amplitude of the small peaks are suppressed. The image on the right, (a2)-(c2), has one A-line, two B-line and one Z-line. The proposed method has one incorrect A-line, whilst HOUGH misses one B-line and the Z-line. The log regulariser of the HOUGH method penalises large values less than the ℓ_1-based penalty, but it diminishes small peaks as it treats them as noises.

For objective evaluation, we tested the performance of our

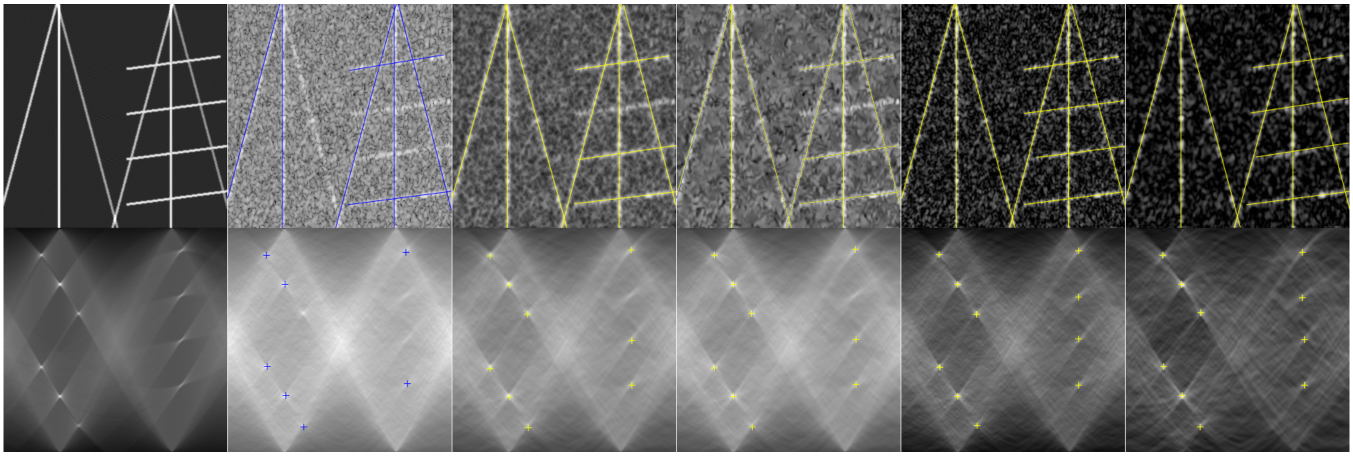

Fig. 2. Line images (top row) and their Radon transform (bottom row), overlaid with lines automatically detected using local maxima. (a) clear line images, (b) B-mode of the simulated speckle y of (a), and the results of (c) STICKS [3], (d) AWBF [12], (e) HOUGH [13] and (f) proposed method x.

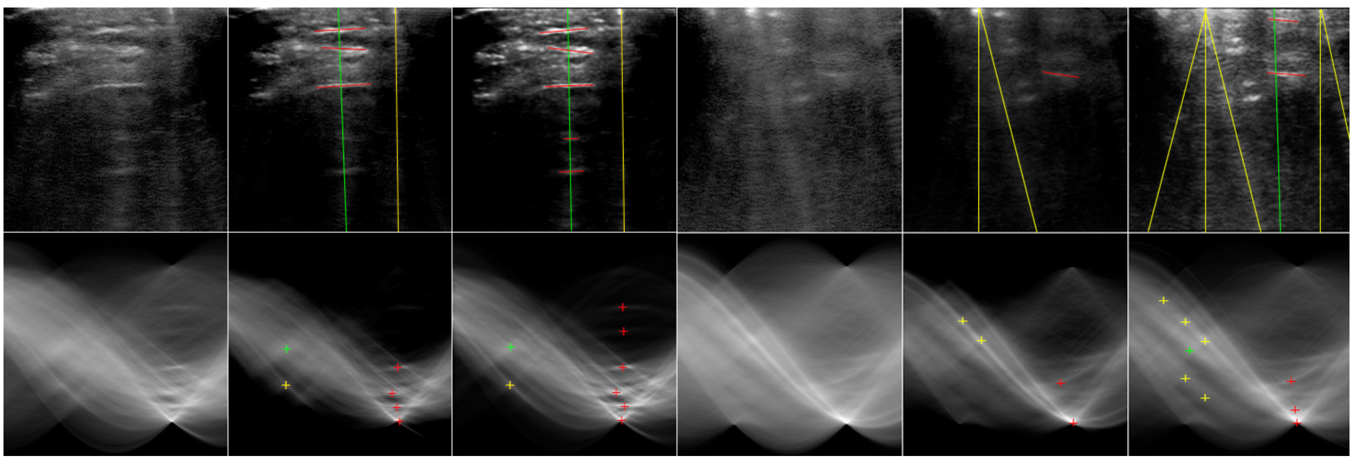

Fig. 3. Lines detected in the lung ultrasounds (top-row) and their Radon transform (bottom-row). (a) original B-mode images, (b) lines detected by HOUGH [13], (c) lines detected by proposed method. The image in (a1-b1-c1) contains one B-line (yellow), one Z-line (green) and five A-lines (red). The image in (a2-b2-c2) contains two B-line (yellow), one Z-line (green) and one A-lines (red).

methods on the B-line detection with 50 lung ultrasound images. Table 1 shows the average results in terms of precision and recall. The precision was computed from the total number of correctly detected B-lines divided by the number of all detected B-lines. The recall was computed from the total number of correctly detected B-lines divided by the total number of the true B-lines. The results show that our proposed method outperforms the STICKS and HOUGH by approximately 30 % and 10 %, respectively.

Table 1. B-line detection performance

method	STICKS [3]	HOUGH [13]	proposed
Precision	0.72	0.92	**0.93**
Recall	0.54	0.62	**0.74**

4. CONCLUSION

This paper presents a novel line detection method using ℓ_1 regularisation. The proposed method restores the lines by solving an inverse problem based on the Radon transform. The method offers a simple and fast implementation via the ADMM by dividing a large problem into a series of subproblems. The proposed method thus achieves line restoration and deconvolution simultaneously. The subjective results show accurately restored lines and the objective results show that the proposed method outperforms existing ones for B-line detection in lung ultrasound imags by up to 30 %.

5. ACKNOWLEDGMENT

We would like to thank Dr. A. Basarab, University Paul Sabatier Toulouse, for the code for simulating images.

6. REFERENCES

[1] A. Achim, A. Bezerianos, and P. Tsakalides, "Novel Bayesian multiscale method for speckle removal in medical ultrasound images," *IEEE Transactions on Medical Imaging*, vol. 20, no. 8, pp. 772–783, Aug 2001.

[2] J.-W. Lee and I.-S. Kweon, "Extraction of line features in a noisy image," *Pattern Recognition*, vol. 30, pp. 1651–1660, 1997.

[3] R. N. Czerwinski, D. L. Jones, and W. D. O'Brien, "Detection of lines and boundaries in speckle images – application to medical ultrasound," *IEEE Transactions on Medical Imaging*, vol. 18, no. 2, pp. 126–136, Feb 1999.

[4] W. Gao, X. Zhang, L. Yang, and H. Liu, "An improved sobel edge detection," in *IEEE International Conference on Computer Science and Information Technology (ICCSIT)*, Jul 2010, vol. 5, pp. 67–71.

[5] M. Allinovi, M.A. Saleem, O. Burgess, C. Armstrong, and W. Hayes, "Lung ultrasound: a novel technique for detecting fluid overload in children on dialysis," *Nephrol. Dial. Transplant.*, 2016.

[6] S. Boyd, N. Parikh, E. Chu, B. Peleato, and J. Eckstein, "Distributed optimization and statistical learning via the alternating direction method of multipliers," *Foundations and Trends in Machine Learning*, vol. 3, no. 1, pp. 1–122, 2011.

[7] N. Anantrasirichai, M. Allinovi, W. Hayes, and A. Achim, "Automatic B-line detection in paediatric lung ultrasound," in *IEEE International Ultrasonics Symposium (IUS)*, 2016.

[8] B. T. Kelley and V. K. Madisetti, "The fast discrete Radon transform: I. Theory," *IEEE Transactions on Image Processing*, vol. 2, no. 3, pp. 382–400, Jul 1993.

[9] N. Parikh and S. Boyd, "Proximal algorithms," *Foundations and Trends in Optimization*, vol. 1, no. 3, pp. 123–231, 2014.

[10] J. M. Bioucas-Dias and M. A. T. Figueiredo, "A new TwIST: Two-step iterative shrinkage/thresholding algorithms for image restoration," *IEEE Transactions on Image Processing*, vol. 16, no. 12, pp. 2992–3004, Dec 2007.

[11] Z. Chen, A. Basarab, and D. Kouamé, "Compressive deconvolution in medical ultrasound imaging," *IEEE Transactions on Medical Imaging*, vol. 35, no. 3, pp. 728–737, 2016.

[12] N. Anantrasirichai, L. Nicholson, J. E. Morgan, I. Erchova, K. Mortlock, R. V. North, J. Albon, and A. Achim, "Adaptive-weighted bilateral filtering and other pre-processing techniques for optical coherence tomography," *Computerized Medical Imaging and Graphics*, vol. 38, no. 6, pp. 526–539, Sep 2014.

[13] N. Aggarwal and W. C. Karl, "Line detection in images through regularized Hough transform," *IEEE Transactions on Image Processing*, vol. 15, no. 3, pp. 582–591, Mar 2006.

[14] O. V. Michailovich and A. Tannenbaum, "Despeckling of medical ultrasound images," *IEEE Transactions on Ultrasonics, Ferroelectrics, and Frequency Control*, vol. 53, no. 1, pp. 64–78, Jan 2006.